SELECTION OF TRANSVERSE DIAGNOSTICS TO MEASURE FEW-MICRON BEAM MODULATIONS IN THE NANOPATTERNED MICROBUNCHING EXPERIMENT*

R. Margraf-O'Neal†, A. Ody, J. Power, Argonne National Laboratory, Lemont, United States
J. Maxson, Cornell University, Ithaca, United States
R. Ryne, Lawrence Berkeley National Laboratory, Berkeley, United States
H. Xu, N. Yampolsky, Los Alamos National Laboratory, Los Alamos, United States
G. Ha, B. N. Temizel Ozdemir, Northern Illinois University, DeKalb, United States
A. Halavanau, N. Majernik, SLAC National Accelerator Laboratory, Menlo Park, United States
G. Andonian, J. Phillips, J. Rosenzweig, University of California, Los Angeles, United States
D. Abell, University of Maryland, College Park, College Park, United States

Abstract

A nanopatterned microbunching collaboration has been formed to test the production of electron microbunches by rotating transverse beamlets into the longitudinal plane using the emittance exchange (EEX) beamline of the Argonne Wakefield Accelerator (AWA). This mechanism has been suggested, such as by the Compact X-ray Free-Electron Laser (CXFEL) group at Arizona State University, to hold the potential to make short-wavelength free-electron lasers (FELs) more compact. Our collaboration will pattern AWA's 44 MeV electron beam with a TEM grid to produce micro-scale beamlets that will become mico-to-nano scale microbunches in the longitudinal plane. Characterizing an array of beamlets with a modulation period at the few micron scale and a low, single pC scale total charge presents challenges in achieving the necessary transverse resolution and signal strength. These proceedings will detail the diagnostics explored to characterize these transverse modulations. We will discuss the merits and challenges of each approach in relation to our application, and progress towards demonstrating these desired diagnostics.

INTRODUCTION

The nanopatterned microbunching experiment [1, 2] is sketched in Fig. 1. 44 MeV electrons are scattered by a 12.5 µm TEM grid, creating transverse beamlets that are then demagnified with quadrupoles [3] to 3 µm, and converted through emittance exchange to 800 nm microbunching.

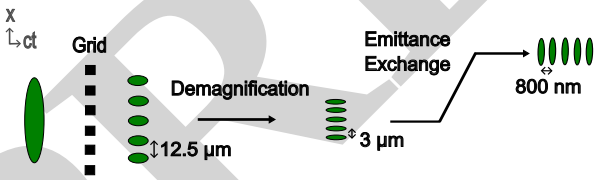

Figure 1: Nanopatterned microbunching experiment.

To tune the quadrupole demagnifier, we need to characterize the micron-scale transverse beamlet pattern after demagnification. However, resolving a single or sub-micron patterned electron beam at 44 MeV is non-trivial. Figure 2 shows a focused 44 MeV electron beam at AWA on a 100 µm thick YAG:Ce screen. The imaging system (BFLY-PGE-23S6M-C Blackfly camera and Nikon AF FX 200mm f/4D IF-ED Lens, with a 381 mm extension between the lens and camera) had 1.3 µm/pixel, and 6.2 µm resolution as measured on a USAF target. However, the smallest RMS beam size measured was $\sigma = 40$ µm. This large size may be due to a blurring of the beam from the YAG:Ce screen, YAG saturation from high charge intensity, an inability to focus the beam to a smaller spot, or a combination of effects.

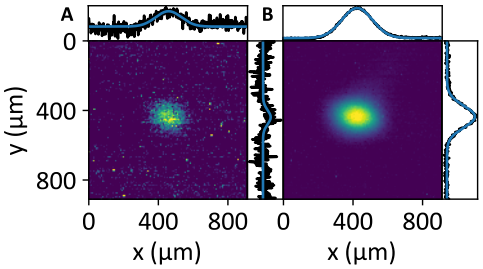

Figure 2: Electron beam measurements at AWA on a 100 µm thick YAG:Ce screen. A) 0.3 pC beam charge, $\sigma_x = 74$ µm, $\sigma_y = 40$ µm, B) 3 pC beam charge, $\sigma_x = 88$ µm, $\sigma_y = 62$ µm.

To better understand this system, we reviewed the literature for high-resolution transverse electron beam diagnostics measuring beams similar to our 44 MeV, ≈1 pC beam. This proceedings will summarize our investigation of transverse diagnostic methods and their applicability to the nanopatterned microbunching experiment.

RESOLVING MEV-SCALE BEAMS

Table 1 presents several examples of high-resolution transverse diagnostics catered towards our goal of measuring a 3 µm modulation at 44 MeV and 1 pC. Since our goal is to measure a patterned beam, not a single beam, resonant cavity beam position monitors have been excluded.

Screen Methods

Screen-based diagnostics provide single-shot 2D profiles.

* This work is supported by the U. S. Department of Energy, under contract No. DE-AC02-06CH11357.
† rmargrafoneal@anl.gov

Table 1: Smallest Beams Measured by a Sample of High-Resolution Transverse Electron Beam Diagnostics

Method	Material	Beam Size, σ (μm)	Energy (MeV)	Charge (pC)	Facility	Refs
Scintillator	YAG:Ce, 20 µm thick	5	8	0.02	UCLA Pegasus	[4]
	YAG:Ce, 100 µm thick	15	7-250	6	PSI SITF	[5], f47
	YAG:Ce, 200 µm thick	14	7	<1	PSI SITF	[6–9]
	LYSO, 200 µm thick	1.4	855	250 pA CW	JGU MAMI	[10]
OTR	Al-coated mirror	14	50	250	BNL-ATF	[11]
	Al-coated Si	0.75	1280	1600	KEK ATF2	[12]
Wire Scan	Au, 900 nm wide	0.434	300	<1	PSI SwissFEL	[13, 14]
	Au, 1 micron wide	2	50–155	0.2	DESY ARES	[15]
Slit Scan	W, 10 µm wide slit	≈50	20	250	DESY PITZ	[16]
Knife-Edge Scan	Si, coated	0.0015 *	0.1	0.2 nA CW	NTT Corp (Lithography)	[17]
	SiN and Au film	0.4	0.75	200 fA CW	LBNL HiRES	[18]
	"Metal"	3.9	4.2	0.0015	SLAC UED	[19]
Moire	Ni mesh	15†	0.003	–	SZU (Vacuum Tube)	[20]

* σ = FWHM/$(2\sqrt{2\ln 2})$ for Gaussian

† σ = FW/$(2\sqrt{3})$ for flat-top

Scintillators Scintillation screens produce light from interaction with high-charged particles. Single-crystal scintillators such as YAG:Ce, LYSO:Ce, LuAG:Ce and YAP:Ce are often thinned to 100s of µm, as at low energies, the thickness of the scintillator directly affects the resolution. This effect can be estimated with the formula for multiple Coulomb scattering [21] (Eqns 34.16 and 34.20):

$$\theta_{rms} = \frac{13.6MeV}{\beta pc} z \sqrt{\frac{x}{X_0}} \left[1 + 0.038 \ln\left(\frac{x}{X_0}\right)\right], \quad (1)$$

where $y_{rms} = d\theta_{rms}/\sqrt{3}$ is resolution, θ_{rms} is the angular distribution, d, X_0 are material thickness and radiation length, and βc, p and z/e are velocity, momentum and charge. For YAG:Ce (X_0 =3.533 cm), this is plotted in Fig. 3. Using this formula, the best resolution expected in Fig. 2 is 0.7 µm, although the achieved resolution is worse. Thinner screens or higher beam energies would improve resolution.

Optical Transition Radiation (OTR) OTR screens produce light as charged particles cross into a material with a different refractive index. A high-resolution example of OTR was performed at 50 MeV [11], suggesting feasibility of OTR measurements at 44 MeV, and achieved a resolution of 14 µm. However, the two-lobed structure of the OTR radiation, which is on the 5-10 µm scale [12], requires careful fitting to resolve sub-10 µm beam sizes, which may be challenging for our sub-micron beamlet array.

Occlusion Scanning Methods

Occlusion-based multi-shot scans move a feature across a beam and collect transmitted or scattered beam/radiation. Resolution, determined by feature and scanning step size, can be higher than screens, with scanning steps <100 nm quite achievable (e.g. AWA owns actuators, Huntington Mechanical Labs, L-2252-6-ESMNC, that microstep ≈63 nm).

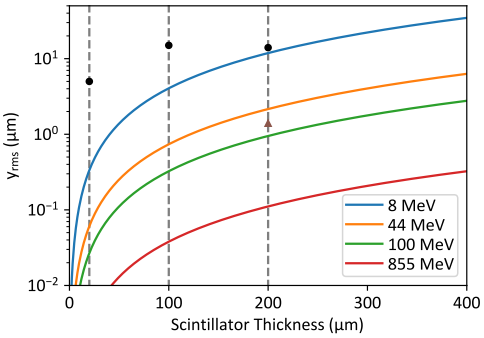

Figure 3: Electron resolution limit on a YAG:Ce screen. Screen thicknesses of 20 µm, 100 µm, and 200 µm are indicated by dashed lines. Markers give examples from Table 1.

Wire Scans A wire scan moves a thin wire across a beam. Downstream detectors measure either electrons scattered by the wire [13, 22], or secondary particles/radiation [15]. Following Equation 1, electron scattering angles are inversely proportional to energy, so measuring the scattered beam is only possible at low energies.

For a 44 MeV beam with 50 nm*rad normalized emittance and transverse beam size is ≈50 µm, beamlet angular divergence at a waist is ≈12 µrad. A 1 µm gold (X_0 = 3.344 mm) wire [15], would produce a scattering angle of 3.7 mrad, much larger than the beam divergence. Thus, at a distance of 5 cm, the scattered beam would be ≈200 µm, while the transmitted beam has expanded negligibly, allowing us to cleanly differentiate the scattered beam from the direct beam. However, the scattered signal may be quite weak. AWA previously measured a 1 pC beam spread out over $FW \approx 500$ µm [2], but larger or weaker beams become drowned by dark current in our beamline, and the beam scattered by a thin wire may be 1% of this signal or less.

Gated cameras can reduce the dark current background, but are expensive. We could instead measure the direct beam, but a detector with high enough dynamic range to measure a small intensity reduction on the direct beam is also costly.

Slit Scans A slit scan moves a thin slit across a beam. Electrons not transmitted by the slit are scattered, and the transmitted beam intensity is measured on a downstream screen or detector [16]. Slit scans are commonly used as part of electron beam emittance measurements, but typically, larger, 100 µm slits are used, and we could not find literature examples where slits were used to measure beams smaller than 50 µm. We suspect this absence is due to slit scans becoming impractical at high energies. At high energy, the electron scattering angle can be smaller than the electron beam divergence, making it difficult to separate the scattered beam or backgrounds from the direct beam.

Slit scans seem feasible at 44 MeV. Consider a 1 µm slit in 3 µm Ni foil, with a 5 µm slit in 12.7 µm stainless steel slit backing (National Aperture, Inc, #2-1-1+HS). The Ni foil (X_0 = 14.24 mm), and steel (for Fe, X_0 = 17.57 mm) will have scattering angles of ≈2 mrad-6 mrad, making the scattered beam easily separable from the direct beam. However, unlike the wire scan, most of the beam is scattered, reducing the dynamic range needed to measure the direct beam.

Since most of the beam is scattered, we also need to consider backgrounds - bremsstrahlung, optical transition radiation (OTR) and Optical Diffraction Radiation (ODR). Fortunately, in the far field, all three effects will be distributed into an angle of $\approx \frac{1}{\gamma}$ = 11 mrad, easy to separate from the direct beam [12, 23, 24], and are estimated to be small. For the slit considered, the photon rate for Bremsstrahlung, $N = \frac{d}{X_0}(\frac{4}{3}\ln\frac{k_{max}}{k_{min}} - \frac{4(k_{max}-k_{min})}{3E} + \frac{k_{max}^2-k_{min}^2}{2E^2}) < .1\%$ [21], even considering a large range of photon kinetic energies (k_{min} =1 eV, k_{max} =100 keV) and neglecting absorption in the material. For OTR, with plasma energy $\hbar\omega_p \approx 60$ eV the photon rate at energies above $\hbar\omega_0$ =1 eV is $N(\hbar\omega > \hbar\omega_0) = \frac{\alpha}{\pi}\left[\left(\ln\frac{\gamma\hbar\omega_p}{\hbar\omega_0} - 1\right)^2 + \frac{\pi^2}{12}\right] \approx 10\%$ [21], unlikely to be overwhelming. ODR becomes similar to OTR radiation when $\lambda << \frac{2\pi a}{\gamma}$. For slit width a =1 µm, $\frac{2\pi a}{\gamma}$ =80 nm at our energy. So UV photons which could be detected by the scintillator may be produced at a similar rate to ODR.

Knife-Edge Scans A knife-edge scan moves the edge of a scattering material across a beam. This method is popular for low energy beams [17–19], and shows no fundamental limits preventing its use at 44 MeV. However, it shares similar problems to the wire scan for signal detection, requiring a large dynamic range to measure the signal of the direct beam from its blocked to fully un-blocked position.

TEM Grid Scans A TEM grid scan moves a grid across a beamlet array, producing high signal contrast when the period of the beamlet array matches the grid. However, since it is a multi-shot measurement which requires a precise match of the TEM grid to beamlet size, it is also a less general-purpose solution.

Moiré Patterns

Moiré patterns are long-wavelength features which form when two periodic structures are overlaid. Electron beam moiré has been shown at 3 keV [20], where a grid of electron beamlets with spacing λ=106 µm scattered off a λ'=106 µm grating (rotated at angle α) to produce features as large as $\lambda_m = \frac{\lambda\lambda'}{\sqrt{\lambda'^2\sin\alpha^2+(\lambda'\cos\alpha-\lambda)^2}}$ = 1.4 mm.

Electron beam moiré could be a fast, single-shot method to show periodicity of a beamlet array. If our beamlet array is incident on an array of similar periodicity, moiré fringes may be produced at long wavelengths resolvable on the YAG:Ce screen. As shown in Fig. 4, a 3 µm pattern offset at 3° produces moiré fringes with λ_m =60 µm.

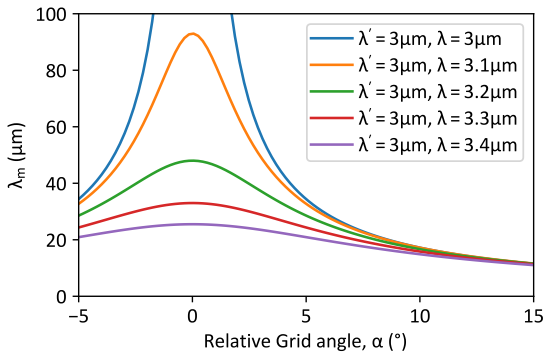

Figure 4: Moiré pattern feature sizes for beamlet spacing λ, grid period λ' and relative angle α.

For effectiveness, grid periodicity must be very close to the beamlet spacing. As shown in Fig. 4, at 0.4 µm (13%) difference between the grid and beamlet spacing, maximum λ_m=25 µm. At larger differences, moiré features become even smaller, until they are no longer resolvable on the screen. Thus, periodicity must match at the ≈10% level.

Single-micron-scale grids are obtainable (e.g. Electron Microscopy Sciences, AUFT306-50, λ' =1.6 µm), making this technique seem feasible. Studying second-order moiré could also determine if this method can work with beamlets more finely spaced than we can obtain TEM grids for.

DISCUSSION/CONCLUSION

After reviewing these options, we are focusing on screen-based diagnostics (20 µm thick YAG:Ce) for resolving beamlets σ >5 µm, and slit and knife-based scans for resolving features σ = 1-5 µm. In tuning the demagnification stage shown in Fig. 1, we will first create beamlets with coarser grids. For example, a grid with 125 µm pitch (Ted Pella, Inc G200G) will produce beamlets with a period of 30 µm after demagnification. These can be resolved on the thin YAG:Ce screen for fast initial tuning. The coarse grids will be subsequently removed and replaced with the finer grids (Ted Pella, Inc G2000HSG) to produce the final 3 µm pattern, which will then be probed with a slower slit or knife-scan.

The thin YAG:Ce and slit and knife-scan diagnostics will be tested in our run in Fall 2026, demonstrating a key requirement of the nanopatterned microbunching experiment.

REFERENCES

[1] G. Ha *et al.*, "Coherent radiation from initially modulated beams using emittance exchange at the Argonne Wakefield Accelerator", *Nucl. Instrum. Methods Phys. Res., Sect. A*, vol. 1075, p. 170387, Jun. 2025. doi:10.1016/j.nima.2025.170387

[2] R. Margraf-O'Neal *et al.*, "Low-charge, high-resolution beamline preparation for the nanopatterned microbunching experiment at argonne wakefield accelerator", in *Proc. NAPAC'25*, Sacramento, CA, USA, pp. 173–176, Aug. 2025. doi:10.18429/JACoW-NAPAC2025-MOP055

[3] B. T. Ozdemir and G. Ha, "Start-to-end simulations of nanometer-emittance beam transport through an emittance exchange beamline", in *Proc. NAPAC'25*, Sacramento, CA, USA, pp. 588–591, Aug. 2025. doi:10.18429/JACoW-NAPAC2025-TUP092

[4] J. Maxson, D. Cesar, G. Calmasini, A. Ody, P. Musumeci, and D. Alesini, "Direct Measurement of Sub-10 fs Relativistic Electron Beams with Ultralow Emittance", *Phys. Rev. Lett*, vol. 118, no. 15, p. 154802, Apr. 2017. doi:10.1103/PhysRevLett.118.154802

[5] T. Schietinger *et al.*, "Commissioning experience and beam physics measurements at the SwissFEL Injector Test Facility", *Phys. Rev. Accel. Beams*, vol. 19, no. 10, p. 100702, Oct. 2016. doi:10.1103/PhysRevAccelBeams.19.100702

[6] R. Ischebeck *et al.*, "Profile Monitors for the SwissFEL Injector Test Facility", in *Proc. LINAC'10*, Tsukuba, Japan, paper TUP103, pp. 656–658, 2010. https://proceedings.jacow.org/LINAC2010/papers/tup103.pdf

[7] R. Ischebeck, "Scintillators for SwissFEL: Usage of Scintillators at the SwissFEL Injector Test Facility", in *Scintillating Screen Applications in Beam Diagnostics Workshop*, Darmstadt, Germany, 2011. https://www-bd.gsi.de/ssabd/contributions/RasmusIschebeck_Scintillators_for_SwissFEL_ScintillatorWorkshop2011.pdf

[8] R. Ischebeck, E. Prat, V. Thominet, and C. Ozkan Loch, "Transverse profile imager for ultrabright electron beams", *Phys. Rev. Spec. Top. Accel. Beams*, vol. 18, no. 8, p. 082802, Aug. 2015. doi:10.1103/PhysRevSTAB.18.082802

[9] R. Ischebeck *et al.*, "Transverse profile monitors for SwissFEL", in *Proc. IBIC2014*, Monterey, CA, USA, paper MOPF31, pp. 119–123, 2014. http://jacow.org/IBIC2014/papers/mopf31.pdf

[10] G. Kube *et al.*, "Transverse Beam Profile Imaging of Few-Micrometer Beam Sizes Based on a Scintillator Screen", in *Proc. IBIC'15*, Melbourne, Australia, Sep. 2015, pp. 330–334, 2015. doi:10.18429/JACoW-IBIC2015-TUPB012

[11] A. Murokh, J. B. Rosenzweig, I. Ben-Zvi, X. J. Wang, and V. Yakimenko, "Limitations on Measuring a Transverse Profile of Ultra-Dense Electron Beams with Scintillators", in *Proc. PAC'01*, Chicago, IL, USA, Jun. 2001, paper TPAH049, pp. 1333–1335, 2001. https://jacow.org/p01/papers/TPAH049.pdf

[12] B. Bolzon *et al.*, "Very high resolution optical transition radiation imaging system: Comparison between simulation and experiment", *Phys. Rev. Spec. Top. Accel. Beams*, vol. 18, no. 8, p. 082803, Aug. 2015. doi:10.1103/PhysRevSTAB.18.082803

[13] GL. Orlandi *et al.*, "Nanofabricated free-standing wire scanners for beam diagnostics with submicrometer resolution", *Phys. Rev. Accel. Beams*, vol. 23, no. 4, p. 042802, Apr. 2020. doi:10.1103/PhysRevAccelBeams.23.042802

[14] G. L. Orlandi *et al.*, "Design and Test of Wire-Scanners for SwissFEL", in *Proc. FEL'14*, Basel, Switzerland, Aug. 2014, paper THP091, pp. 948–951, 2014. https://jacow.org/FEL2014/papers/THP091.pdf

[15] M. Maxton, "Determining the emittance using a wire scanner", *DESY Summer Student Report*, 2022. https://www.desy.de/f/students/2022/reports/Marleen.Maxton.pdf

[16] L. Staykov, "Design optimization of an emittance measurement system at pitz", in *DIPAC'05*, Jun. 2005. http://accelconf.web.cern.ch/d05/PAPERS/POT032.pdf

[17] K. Yamazaki and H. Namatsu, "Electron-Beam Diameter Measurement Using a Knife Edge with a Visor for Scattering Electrons", *Jpn. J. Appl. Phys.*, vol. 42, no. Part 2, No. 5A, pp. L491–L493, May 2003. doi:10.1143/JJAP.42.L491

[18] F. Ji, D. B. Durham, A. M. Minor, P. Musumeci, J. G. Navarro, and D. Filippetto, "Ultrafast Relativistic Electron Nanoprobes", *Commun. Phys*, vol. 2, no. 1, p. 54, May 2019. doi:10.1038/s42005-019-0154-4

[19] X. Shen *et al.*, "Femtosecond mega-electron-volt electron microdiffraction", *Ultramicroscopy*, vol. 184, pp. 172–176, Jan. 2018. doi:10.1016/j.ultramic.2017.08.019

[20] Y. Lei, Y. Liao, J.-h. Long, H. Cai, Y. Bai, and J. Liu, "Observation of electron beam moiré fringes in an image conversion tube", *Ultramicroscopy*, vol. 170, pp. 19–23, Nov. 2016. doi:10.1016/j.ultramic.2016.07.013

[21] S. Navas *et al.*, "Review of particle physics", *Phys. Rev. D*, vol. 110, no. 3, p. 030001, 2024. doi:10.1103/PhysRevD.110.030001

[22] C. O. Loch, D. L. Sancho, P. Pollet, G. Marinkovic, R. Ischebeck, and V. Schlott, "System Integration of SwissFEL Beam Loss Monitors", in *Proc. IBIC'15*, Melbourne, Australia, Sep. 2015, pp. 170–174, 2015. doi:10.18429/JACoW-IBIC2015-MOPB051

[23] H. Bethe and W. Heitler, "On the Stopping of Fast Particles and on the Creation of Positive Electrons", *Proc. R. Soc. London, Ser. A*, vol. 146, no. 856, pp. 83–112, 1934. http://www.jstor.org/stable/2935479

[24] A. P. Potylitsyn, M. I. Ryazanov, M. N. Strikhanov, and A. A. Tishchenko, *Diffraction Radiation from Relativistic Particles*. Berlin, Heidelberg: Springer Berlin Heidelberg, 2011. doi:10.1007/978-3-642-12513-3